

DETECTION OF THE UNIVERSAL EFFECT OF THE LARGE SCALE VELOCITY SHEAR ON THE INFALL DIRECTIONS OF THE GALACTIC SATELLITES

Jounghun Lee¹, Yun-Young Choi²

ABSTRACT

We report a detection of the universal effect of the large-scale velocity shear on the infall directions of the galactic satellites into their hosts. Identifying the isolated galactic systems each of which consists of a single host galaxy and its satellites from the Seventh Data Release of the Sloan Digital Sky Survey Data and using the velocity shear field recently reconstructed by Lee et al. in the local universe, we investigate the alignments between the relative positions of the satellites from their isolated hosts and the principal axes of the local velocity shear tensors. We find a clear signal that the galactic satellites in isolated systems are located preferentially along the directions of the minor principal axes of the local velocity shears smoothed on the scale of $10 h^{-1}\text{Mpc}$. Those galactic satellites which are fainter and located at larger distances from the hosts are shown to yield stronger alignments. It is also shown that the alignment strength is quite insensitive to the cosmic web environment as well as to the luminosity, mass, richness and morphology of the isolated hosts and their satellites, which is consistent with the recent prediction of Libeskind et al. based on a N -body experiment that the velocity shear effect on the satellite infall direction is universal.

Subject headings: galaxies:clusters — large scale structure of universe

1. INTRODUCTION

The filamentary distributions of the galaxies and the web-like interconnections between the structures over different scales are collectively called the cosmic web phenomenon. The

¹Astronomy Program, Department of Physics and Astronomy, Seoul National University, Seoul 151-747, Korea; jounghun@astro.snu.ac.kr

²Department of Astronomy and Space Science, Kyung Hee University, Gyeonggi 446-701, Korea; yy.choi@khu.ac.kr

recent observations have disclosed the ubiquitous appearance of the cosmic web phenomena (e.g., Jones et al. 2009; Abazajian et al. 2009; Huchra et al. 2012), which agrees with the numerical results from N -body simulations for a standard Λ CDM cosmology where the energy density of the universe is contributed dominantly by the cosmological constant Λ and the collisionless Cold Dark Matter (e.g., Bond et al. 1996; Springel et al. 2005). An urgently requested task in the field of the large scale structure is to find a tracer of the cosmic web with which the complicated filamentary pattern in the cosmic web can be coherently described and the key mechanism for the web interconnection can be quantitatively understood.

The velocity shear field proposed by Hoffman et al. (2012) as an efficient diagnostic of the web environment has recently drawn exploring attention. They suggested that the cosmic environments be readily classified into the four standard categories (i.e., knot, filament, sheet, void) by putting some non-zero threshold on the three eigenvalues of the local velocity shear tensor and demonstrated with a high-resolution N -body simulation that the web environments classified by their algorithm reproduced very well the expected images of the four categories.

It is worth mentioning here how the velocity shear field is different from the tidal shear field that was widely used as a tracer of the cosmic web in the previous approaches based on the classical cosmic web theory (e.g., Bond et al. 1996; Hahn et al. 2007; Platen et al. 2008; Lee et al. 2009; Zhang et al. 2009, 2013). The tidal shear field defined as the second derivative of the gravitational potential is basically a linear quantity, obtained under the implicit assumption that the peculiar velocity field is curl free. Whereas, the velocity shear field is an extension of the tidal shear field to the nonlinear regime where the velocity field develops a curl motion. Given that the cosmic web pattern penetrates deep into the nonlinear scales, the velocity shear field should trace better the nonlinear evolution of the cosmic web, being more suitable for the description of the interconnection over widely different scales (Hoffman et al. 2012).

The usefulness of the velocity shear field as a tracer of the cosmic web has been noted by the subsequent numerical studies based on high-resolution N -body experiments. Libeskind et al. (2013a) explained that the alignments between the shapes and angular momentum of the dark matter halos and the large-scale environments must have been mainly caused by the anisotropic gravitational collapse and accretion of dark matter along the principal axes of the velocity shear field. Libeskind et al. (2013b) demonstrated that the web interconnection should be a consequence of the stability of the velocity shear field against the change of the filtering scale. Tempel et al. (2014) showed that the filamentary structures identified in their N -body simulations are indeed elongated along the minor principal axes of the velocity shear field.

Libeskind et al. (2014b) performed a more systematic investigation of the velocity shear effect on the generation of the cosmic web. Noting that the presence of the cosmic web phenomena on all scales essentially implies that there are preferred directions in the occurrence of the accretion and merging events through which the structure formation proceeds in the standard Λ CDM picture, Libeskind et al. (2014b) have shown by their N -body experiments that the infall and accretion events of the satellites always occur along the minor principal axes of the velocity shear field on all scales, no matter what environment the satellites are located and no matter what mass the satellites and hosts have.

These numerical results have provided a theoretical understanding of the strong alignment between the spatial distribution of the satellites and the shapes of their hosts, which were shown by many numerical works based on N -body or hydrodynamic simulations (e.g., Wang et al. 2005; Zentner et al. 2005; Agustsson & Brainerd 2006; Kang et al. 2007; Libeskind et al. 2007; Deason et al. 2011; Wang et al. 2014; Dong et al. 2014). As the accretion of dark matter onto a host occurs along the direction of the minor principal axis of the *small-scale* velocity shear field, the shape of the host becomes elongated along that direction. As the infall of the satellites into the host occurs preferentially along the direction of the minor principal axis of the larger scale velocity shear field, the spatial distributions of the satellites around the host are aligned with that direction. Since the velocity shear field on two different scales are strongly cross-correlated, the shape of a host becomes aligned with the spatial distribution of its satellites (Libeskind et al. 2014b).

Although the alignments between the host shapes and the satellite locations have been supported by several observational studies (e.g., Brainerd 2005; Yang et al. 2006; Azzaro et al. 2007; Bailin et al. 2008; Agustsson & Brainerd 2010, 2011), no direct observational evidence was found for the preferential alignments of the satellite infall directions with the minor principal axes of the velocity shear nor for the strong cross-correlations between the velocity shear field smoothed on different scales. Very recently, Lee et al. (2014) have found a direct observational evidence for the alignment between the infall directions of the satellite galaxies and the minor principal axes of the local velocity shear tensor. Analyzing the spatial distribution of the satellite galaxies around the Virgo cluster from the Extended Virgo Cluster Catalog (EVCC) compiled by Kim et al. (2014) and determining the principal directions of the velocity shear tensor around the Virgo cluster from the peculiar velocity shear field recently reconstructed by Wang et al. (2012), they showed that the satellite galaxies located beyond the virial radius of the Virgo cluster tend to reside in the plane perpendicular to the major principal axes of the local velocity shear tensor.

In their analysis, however, Lee et al. (2014) had to project the positions of the Virgo satellites as well as the principal axes of the local velocity shear tensor onto the plane of

the sky to eliminate the severe effect of nonlinear redshift space distortion expected to be present around the highly overdense Virgo region. Besides, the minor principal axes of the local velocity shear at the Virgo center turned out to be almost perpendicular to the line of sight direction and thus the true three dimensional direction was completely lost during the projection process. In consequence, what Lee et al. (2014) were able to find was not directly the alignments of the Virgo satellites with the minor principal axis of the local velocity shear tensor but their anti-alignments with the major principal axis that lie in the plane of the sky.

In order to find a more direct evidence for the preferential occurrences of the satellite accretion along the minor principal axes of the velocity shear field, it is necessary to consider those systems where the non-linear redshift effect is not severe. An isolated galactic system composed of a single host galaxy and its satellites should be a good target for this study. The nonlinear redshift distortion effect is expected to be less severe around a galaxy than in a cluster. Furthermore, for the case of an *isolated* galactic system, its satellites can be readily identified by analyzing the spatial distributions of the galaxies around it. We attempt here to find a signal of the alignments between the locations of the galactic satellites around the isolated host galaxies and the minor principal axes of the velocity shear tensors measured at the positions of the hosts by analyzing the galaxy catalog from the Seventh Data Release of the Sloan Digital Sky Survey (SDSS DR7) (Abazajian et al. 2009). Unlike in the work of Lee et al. (2014), we will have to take a *statistical approach* rather than focusing on each galactic system since the number of the satellites around an isolated galaxy is much lower than that around a massive cluster like the Virgo cluster.

The plan of this paper is as follows. In section 2, we provide an observational evidence for the alignments between the spatial distributions of the galactic satellites in isolated systems and the minor principal axes of the large-scale velocity shear field. In section 3 we present the results of our investigation of the dependence of the alignment strength on the properties of the galactic satellites as well as on the web environments. In section 4 we discuss the inconsistencies as well as the consistencies of our results with the recent numerical findings and draw a final conclusion. Throughout this Paper, we assume a flat Λ CDM universe whose initial conditions are described by the key cosmological parameters set at the values of $\Omega_m = 0.26$, $\Omega_\Lambda = 0.74$, $h = 0.73$, $\sigma_8 = 0.8$.

2. ALIGNMENTS BETWEEN THE GALACTIC SATELLITES AND THE LARGE-SCALE VELOCITY SHEARS

What we would like to see is if and how strongly the spatial distributions of the galactic satellites in isolated systems are aligned with the principal axes of the large-scale velocity shears estimated at their host positions. For this study, we utilize the velocity shear field which Lee et al. (2014) reconstructed in the local volume by analyzing the peculiar velocity fields that Wang et al. (2012) had reconstructed from the SDSS DR7 group catalogs. The reconstruction was made on a regular box of volume $180^3 h^{-3} \text{Mpc}^3$ consisting of 256^3 pixels. The ranges of the Cartesian coordinates, x , y , z , of the 256^3 pixels in the equatorial reference frame are given in unit of $h^{-1} \text{Mpc}$ as $[-182.29, -1.49]$, $[-90.05, 90.74]$, $[-22.73, 188.07]$, respectively. The velocity shear tensor, (Σ_{ij}) , was evaluated from the peculiar velocity vector, (v_i) according to the definition given in Hoffman et al. (2012) as $\Sigma_{ij} \propto \partial_i v_j + \partial_j v_i$. From here on, the *local volume* means the volume composed of these pixels each of which the velocity shear tensor is assigned. For more detailed explanation about how the velocity shear field was reconstructed in the local volume, the readers are referred to Lee et al. (2014).

We construct a sample of the isolated galactic systems each of which consists of a single host and at least one satellite from the SDSS DR7 spectroscopic datasets (Abazajian et al. 2009) by following the procedure prescribed in Hwang & Park (2010). Focusing on the local volume where the velocity shear field was reconstructed, we select those galaxies as the hosts which are at least one magnitude brighter in the r -band than the survey limit, which amounts to putting a threshold $m_c = 16.77$ as a lower limit on the r -band magnitudes, m_r , of the SDSS galaxies. The fainter galaxies are excluded from our sample since the measurements of their positions are likely to suffer from large uncertainties. The r -band absolute magnitude, M_r , of each selected galaxy as an isolated host is calculated from m_r by properly taking into account both of the K -correction (Blanton et al. 2003) and the luminosity evolution correction (Tegmark et al. 2004).

For each host with $m_r \geq m_c$, we look for its nearest neighbor galaxy and determine the difference between the heliocentric velocities of the host and its nearest neighbor along the line of sight, Δv , as well as the tangential separation distance between them in the projected plane of the sky, d_n . As done in Hwang & Park (2010), the host galaxies are identified as the isolated ones if their nearest neighbors satisfy two conditions of $d_n \geq \max\{R_v, R_{vn}\}$ and $\Delta v \geq \Delta v_c$, where R_v and R_{vn} are the tangential virial radii of the host galaxy and its nearest neighbor, respectively, where the virial radius is defined as the projected radius which encloses the mean mass density as high as 200 times the critical density of the universe. We set the threshold value of the velocity difference, Δv_c , at 900km/s and 600km/s for the cases of ellipticals and spirals, respectively (Park & Choi 2009).

Suppose that an isolated host galaxy has the absolute r -band magnitude of M_r . The candidates of its satellites are those galaxies which satisfy the following two conditions. First, the absolute r -band magnitude is larger than $M_r + 1$. Second, the difference in the velocity from the host is smaller than $v_0 10^{-2(M_r+21)/15}$ where $v_0 = 900\text{km/s}$ and 600km/s for ellipticals and spirals, respectively. The true satellites of this isolated host galaxy are identified among the candidates as the ones whose separation distances from the isolated host, d_s , in the projected plane of sky are less than some threshold, d_{sc} , given as

$$d_{sc} = \min \left\{ \frac{d_n R_v}{R_v + R_{nv}}, d_n - R_{nv}, 3 h^{-1}\text{Mpc} \right\}. \quad (1)$$

A total of 10646 SDSS galaxies are selected as the isolated hosts having one or more satellites in the local volume. For the detailed description of how to identify the isolated galactic systems, the readers are referred to Park & Choi (2009) and Hwang & Park (2010).

Figure 1 plots the absolute r -band magnitudes of the isolated host galaxies (black dots) and their satellites (grey dots) from the selected sample of the SDSS DR7 as a function of redshift. Figure 2 illustrates the configuration of the satellites (grey dots) identified around the isolated host galaxies (black cross), whose declination (DEC) and right ascension (RA) belong to the range to $12 \leq \text{DEC} \leq 32$ and $162 \leq \text{RA} \leq 182$ in unit of degree, respectively, with redshifts in the range of $0.02 \leq z \leq 0.03$. The radius of the circle around each isolated host galaxy corresponds to the threshold separation distance, d_{sc} , in Equation (1). For the visibility, only those galactic systems having two or more satellites are shown in Figures 1-2. Table 1 lists the ranges of the absolute r -band magnitude, tangential virial radius, and the mean satellite number of the isolated hosts with one or more satellites within the local volume.

Using information on the equatorial coordinates of the host and its satellite in each of the selected isolated system, we determine the three dimensional (comoving) positions, \mathbf{r}_s , of the satellites relative to the host. At the pixel to which the position of each isolated host belongs, we diagonalize the velocity shear tensor (Σ_{ij}) through the similarity transformation to evaluate its three eigenvalues (say, $\lambda_1, \lambda_2, \lambda_3$ in a decreasing order) and determine the corresponding three eigenvectors (say, $\hat{\mathbf{e}}_1, \hat{\mathbf{e}}_2, \hat{\mathbf{e}}_3$) as the major, intermediate and minor principal axes of the velocity shear tensor. Figure 3 depicts the three dimensional spatial distribution of the galactic satellites (pale grey ellipses) around an isolated host galaxy (dark grey ellipse) in the principal frame of the local velocity shear.

We define the *alignment measure*, μ , of each selected system as the mean value of the cosines of the angles between the relative positions of the satellites and the principal axes of

the local velocity shear tensor

$$\mu_i \equiv \frac{1}{N_s} \sum_{\alpha} \frac{|\mathbf{r}_s^{\alpha} \cdot \mathbf{e}_i|}{|\mathbf{r}_s^{\alpha}| |\mathbf{e}_i|}, \quad \text{for } i = 1, 2, 3, \quad (2)$$

where N_s is the number of the satellites belonging to a given system, \mathbf{r}_s^{α} is the relative three dimensional position of the α -th satellite. If the satellites are isotropically distributed with respect to the principal axes of the velocity shear field, then the alignment measure would be close to 0.5 for $i = 1, 2, 3$. If the satellites are preferentially distributed along the minor principal axes as predicted by Libeskind et al. (2014b), then the alignment measure would exceed 0.5 for $i = 1$ while it drops below 0.5 for $i = 2$ and 3.

Binning the values of the alignment measures from all of the selected galactic systems and counting the numbers, N_{sys} , of the systems whose alignment measures fall into each bin, we calculate the probability density distributions of the alignment measure as $p(\mu_i) = N_{sys}/(N_T d\mu)$ for $i = 1, 2, 3$ where N_T denotes the total number of the selected galactic systems. Figure 4 plots the probability density distributions of the alignment measure for the case that the large-scale velocity shear field smoothed on the scale of $10 h^{-1}\text{Mpc}$. The solid, dashed and dotted lines correspond to the cases of $p(\mu_3)$, $p(\mu_2)$, $p(\mu_1)$, respectively. As can be seen, in the high- μ section ($\mu \geq 0.5$), $p(\mu_3)$ has much higher value than $p(\mu_2)$ and $p(\mu_1)$, while in the low- μ section ($\mu < 0.5$) the trend becomes the opposite. This result explicitly proves that the galactic satellites in the isolated systems are indeed preferentially distributed along the minor principal axes of the large-scale velocity shear field.

To see how the alignment measure changes with the filtering scale R_f of the velocity shear field, we repeat the whole process described above for three different cases: $R_f = 3, 5, 7 h^{-1}\text{Mpc}$. For each case, we take the ensemble average of μ over all the selected systems, the results of which are shown in Figure 5. The dashed, dot-dashed, long-dashed, and solid lines correspond to the cases that the local velocity shear field is smoothed on the filtering scales of 3, 5, 7 and $10 h^{-1}\text{Mpc}$, respectively, while the case of no preferential alignment is shown as dotted line. The first, second and third bins from the left on the horizontal axis correspond to the cases that the alignment measures are calculated with respect to \mathbf{e}_3 , \mathbf{e}_2 and \mathbf{e}_1 , respectively. The errors represent the standard deviation in the measurement of $\langle \mu \rangle$ calculated as $\sqrt{\langle \Delta^2 \mu \rangle / (N_{sys} - 1)}$. As can be seen in Figure 5, the alignment tendency between the satellite positions and the minor principal axes does not disappear as the filtering scale varies. But, it is also clear that the strength of the alignment decreases as R_f decreases. In other words, the relative positions of the satellites are more strongly aligned with the large-scale velocity shear field.

3. DEPENDENCE OF THE ALIGNMENT SIGNAL ON THE PHYSICAL PROPERTIES OF THE SATELLITES

Under the assumption that the directions of the relative positions of the galactic satellites represent well the directions of their infall motions into their hosts, the results of section 2 provides a clear observational evidence that the galactic satellites tend to fall into their hosts in the directions parallel to the minor principal axes of the large-scale velocity shear field. Now, we would like to investigate how the alignment tendency depends on the properties of the galactic systems and to see if it is truly universal as claimed by Libeskind et al. (2014b). Let us first examine if and how the alignment between the satellite positions and the principal axes of the large-scale velocity shears depends on the distances of the satellites from the hosts. From here on, the smoothing scale of the velocity shear field is set at $R_f = 10 h^{-1} \text{Mpc}$. For each selected galactic system, we divide the satellites into two subsamples according to their three dimensional distances r_s from their host. One subsample consists of those satellites with $r_s \geq 2R_v$ while the other has the satellites with $r_s < 2R_v$, where R_v denotes the tangential virial radius of their host. The value of μ of each system is measured twice by using the two subsamples separately.

The top (bottom) panel of Figure 6 shows the ensemble averages of the alignment measures, $\langle \mu \rangle$, for the case that the value of μ of each galactic system is measured by using only those satellites located beyond (within) twice the virial radius of their host. In each panel, the solid and dashed lines correspond to the cases of $R_f = 3 h^{-1}$ and $10 h^{-1}$, respectively. As can be seen, the satellites with $r_s \geq 2R_v$ tend to be much more strongly aligned with the minor principal axes of the local velocity shear for both of the cases of R_f than the satellites with $r_s < 2R_v$. This result implies that the alignment tendency between the infall directions of the satellites with the minor principal axes of the large-scale velocity shear field becomes diminished as the satellites come close to their hosts where the non-linear effect becomes dominant.

Separating the brighter satellites of each galactic system with $M_r \leq M_{r0}$ from the fainter ones with $M_r > M_{r0}$ where $M_{r0} = -18.2$ is the median value of the absolute r -band magnitudes of the satellites of all selected systems, the value of μ of each galactic system is measured twice by using the two subsamples separately. Figure 7 shows the ensemble average of the alignment measure, $\langle \mu \rangle$, for the case that the value of μ of each galactic system is measured by using the brighter (fainter) satellites in the top (bottom) panel, revealing how $\langle \mu \rangle$ depends on the absolute r -band magnitudes of the satellites. Although the fainter galaxies seem to yield slightly stronger signal of alignment than the brighter counterparts, the difference in the alignment tendency between the brighter and the fainter satellites is not so significant. The slightly strong alignment of the fainter galaxies should be caused by

the fact that the fainter galaxies are located at relatively larger distances from the hosts.

We also investigate whether or not the alignment measure depends on the morphology of the satellites. Using the morphology segregator algorithm suggested by Park & Choi (2005), we classify the satellites of each galactic system into the ellipticals and the spirals. Then, the alignment measure of each galactic system is measured twice by using the ellipticals and the spirals separately. Figure 8 displays the results, revealing that the strength of the alignment does not depend on the satellite morphology. The results shown in Figures 7-8 imply that the strength of the alignment between the directions of the infall of the galactic satellites into their hosts and the minor principal axes of the velocity shear field is quite insensitive to the physical properties of the galactic satellites.

Now, we would like to see if and how the alignment strength depends on the properties of the host galaxies as well as on the surrounding environment. After measuring the alignment measure of each galactic system by using all of its satellites, we take an ensemble average over only those systems which have more than one satellites. The same averaging process is repeated but over those systems which have only one satellite. The results are shown in Figure 9 which reveals that the alignment strength is almost the same for the two cases. Since a more massive host would have a larger number of satellites, this result indicates that the alignment strength is almost independent of the masses of the host galaxies. It also suggests that the alignment strength should be insensitive to the environmental density given that the galactic systems located in high-density environments must have more satellites.

To examine how the alignment tendency varies with the size of the host, we first calculate the median value of the tangential virial radii of the selected isolated hosts and find it to be $0.28 h^{-1}\text{Mpc}$. Determining the alignment measure of each galactic system, we calculate the ensemble average of μ only over those systems whose hosts have R_v larger than the median value. We repeat the same but only over those with R_v less than the median value. Figure 10 shows the result, indicating that the alignment strength between the infall directions of the galactic satellites and the minor principal axes of the large-scale velocity shear field is insensitive to the sizes of the host galaxies. We also examine how the alignment strength depends on the morphology of the hosts and find almost no variation.

Using the web-classification scheme suggested by Hahn et al. (2007), we determine in which web environment each galactic system reside and find that most of the systems are located either in the filament where $\lambda_1 \geq \lambda_2 \geq 0$ and $\lambda_3 < 0$ or in the sheet where $\lambda_1 \geq 0$ and $\lambda_2 < 0$. Among the 10646 selected galactic systems, a total of 4975 (4422) systems are found to be in the filament (sheet). The rest of the selected systems are found to reside either in the knot or in the void. After calculating μ of each galactic system, we take its ensemble average over only those systems located in the filament. We repeat the same but

over those systems located in the sheet. We do not consider the galactic systems residing in the void or in the knot since the evaluation of $\langle \mu \rangle$ would suffer from small number statistics for that case. Figure 11 shows how the ensemble average of the alignment measure differs between in the sheet and in the filament environments. As can be seen, there is almost no difference between the two cases. This result shows that the infall events of galactic satellites always occur along the minor principal axes of the large-scale velocity field no matter what environment the galactic systems are located, which is consistent with the numerical prediction of Libeskind et al. (2014b) based on a high-resolution N -body simulations.

4. SUMMARY AND DISCUSSION

In light of the work of Libeskind et al. (2014b) which claimed with the help of a N -body experiment that the preferential occurrence of the infall events of the satellites into their hosts along the minor principal directions of the velocity shear field is an "universal" phenomenon, we have tested this numerical prediction against observational data. Using a sample of the isolated galactic systems from the SDSS DR7 and the velocity shear field recently reconstructed by Lee et al. (2014) in the local universe, we have found an unrefutable observational evidence that the infall directions of the galactic satellites into their isolated hosts indeed occur preferentially along the minor principal axes of the large-scale velocity field smoothed on the scale of $10 h^{-1} \text{Mpc}$. Investigating the dependence of the alignment tendency on the properties of the satellites, properties of the host galaxies, web environments and filtering scale, we have found that the alignment tendency exists for all of the cases considered here, no matter how massive the galactic systems are, no matter what morphological types the satellites and the hosts have, and no matter what environments surround them. Our result provides a first direct observational evidence for the "universal" effect of the velocity shear on the infall directions of the galactic satellites.

It is, however, worth noting that there are some apparent inconsistencies between our result and the numerical prediction. One inconsistency has been shown in the trend of the alignment with the filtering scale. What we have found is that on the scales smaller than $10 h^{-1} \text{Mpc}$, the alignments between the spatial distributions of the galactic satellites and the minor principal axes of the velocity shear field are less strong, which is in direct contrast with the result of the N -body experiment of Libeskind et al. (2014b) who found that the strength of the alignment increases as the scale decreases. The other inconsistency was witnessed in the trend of the alignment strength with the luminosity of the galactic satellites. The numerical experiment showed that the infall directions of the more massive satellites are more strongly aligned with the minor principal axes of the velocity shear field. Whereas our

observational analyses have indicated that the spatial distributions of the galactics satellites with lower luminosity exhibit slightly stronger alignments with the minor principal axes of the velocity shear tensor.

We believe that this apparent inconsistencies may be due to the inaccuracy of the approximation that we have made to determine the principal axes of the velocity shear field and the directions of the satellite infall motions. First, we used the linearly reconstructed velocity shear field which is, strictly speaking, valid only in the linear regime. Although the principal axes of the linearly reconstructed velocity shear field and those of the real velocity shear field align well with one another on large scale with those of the real velocity shear field (Lee et al. 2009; Libeskind et al. 2014a,b), they would deviate substantially from one another on small scales where the nonlinear modification becomes significant. Second, in the numerical work of Libeskind et al. (2014b), they measured accurately the true direction of the accretion of each satellite by tracing its motions at different redshifts. In our observational analysis, however, it was impossible to make such an accurate measurement and thus had to approximate the direction of the infall event of each satellite by that of its relative position from the host. Another possible cause for the inconsistency is the difference in the locations of the galactic systems. In our observational analysis, we restrict our attention only to the *isolated* galactic systems given that the satellites of the isolated systems can be readily identified. Our result may imply that for the cases of the isolated galactic systems, the infall directions of the satellites trace better the principal axes of the *large-scale* velocity shear field than the small-scale counterparts. A numerical confirmation of this explanation will be necessary in the future.

It should be also worth recalling the previous numerical works (e.g, Sales & Lambas 2004; Bailin et al. 2008; Dong et al. 2014) which found that the preferential alignments with the major axes of the host galaxies were exhibited only by the elliptical satellites but not by the spiral counterparts and comparing it with our result that the alignment between the infall directions of the satellites and the minor principal axes of the large-scale velocity shear field is independent of the morphology of the satellites. This comparison leads us to the following interpretation. (i) The infall and accretion of the satellites always occur along the minor principal axes of the large-scale velocity shear field, no matter what morphology they have. (ii) Upon the completion of the infall of the satellites into the host galaxies, their locations come to be modified by the nonlinear effects which include the generation of the curl motions of the velocity field within the virial radii of the host galaxies. (iii) The alignments between the elongated axes of the hosts and the locations of their satellites are modulated dominantly by the non-linear effect after the infall, resulting in the dependence of the alignment strength on the galaxy morphology as well as on the assembly history.

Funding for the SDSS and SDSS-II has been provided by the Alfred P. Sloan Foundation, the Participating Institutions, the National Science Foundation, the U.S. Department of Energy, the National Aeronautics and Space Administration, the Japanese Monbukagakusho, the Max Planck Society, and the Higher Education Funding Council for England. The SDSS Web Site is <http://www.sdss.org/>.

The SDSS is managed by the Astrophysical Research Consortium for the Participating Institutions. The Participating Institutions are the American Museum of Natural History, Astrophysical Institute Potsdam, University of Basel, University of Cambridge, Case Western Reserve University, University of Chicago, Drexel University, Fermi lab, the Institute for Advanced Study, the Japan Participation Group, Johns Hopkins University, the Joint Institute for Nuclear Astrophysics, the Kavli Institute for Particle Astrophysics and Cosmology, the Korean Scientist Group, the Chinese Academy of Sciences (LAMOST), Los Alamos National Laboratory, the Max-Planck-Institute for Astronomy (MPIA), the Max-Planck-Institute for Astrophysics (MPA), New Mexico State University, Ohio State University, University of Pittsburgh, University of Portsmouth, Princeton University, the United States Naval Observatory, and the University of Washington.

J.L. thanks H. Wang for providing the dataset of the peculiar velocity field. This work was supported by the research grant from the National Research Foundation of Korea to the Center for Galaxy Evolution Research (NO. 2010-0027910). J.L. also acknowledges the financial support by the Basic Science Research Program through the National Research Foundation of Korea (NRF) funded by the Ministry of Education (NO. 2013004372).

REFERENCES

Abazajian, K. N., Adelman-McCarthy, J. K., Agüeros, M. A., et al. 2009, *ApJS*, 182, 543

Agustsson, I., & Brainerd, T. G. 2006, *ApJ*, 650, 550

Agustsson, I., & Brainerd, T. G. 2010, *ApJ*, 709, 1321

Agustsson, I., & Brainerd, T. G. 2011, *ISRN Astronomy and Astrophysics*, 2011, 958973 [arXiv:1110.5920]

Ann, H. B., Park, C., & Choi, Y.-Y. 2008, *MNRAS*, 389, 86

Azzaro, M., Patiri, S. G., Prada, F., & Zentner, A. R. 2007, *MNRAS*, 376, L43

Bailin, J., Power, C., Norberg, P., Zaritsky, D., & Gibson, B. K. 2008, *MNRAS*, 390, 1133

Blanton, M. R., Eisenstein, D., Hogg, D. W., Schlegel, D. J., & Brinkmann, J. 2003, *AJ*, 125, 2348

Bond, J. R., Kofman, L., & Pogosyan, D. 1996, *Nature*, 380, 603

Brainerd, T. G. 2005, *ApJ*, 628, L101

Deason, A. J., McCarthy, I. G., Font, A. S., et al. 2011, *MNRAS*, 415, 2607

Dong, X., Lin, W., Kang, X., et al. 2014, arXiv:1407.6708

Forero-Romero, J. E., Hoffman, Y., Gottlöber, S., Klypin, A., & Yepes, G. 2009, *MNRAS*, 396, 1815

Hwang, H. S., & Park, C. 2010, *ApJ*, 720, 522

Forero-Romero, J. E., Contreras, S., & Padilla, N. 2014, arXiv:1406.0508

Hahn, O., Porciani, C., Carollo, C. M., & Dekel, A. 2007, *MNRAS*, 375, 489

Hoffman, Y., Metuki, O., Yepes, G., et al. 2012, *MNRAS*, 425, 2049

Huchra, J. P., Macri, L. M., Masters, K. L., et al. 2012, *ApJS*, 199, 26

Hwang, H. S., & Park, C. 2010, *ApJ*, 720, 522

Jones, D. H., Read, M. A., Saunders, W., et al. 2009, *MNRAS*, 399, 683

Kang, X., van den Bosch, F. C., Yang, X., et al. 2007, *MNRAS*, 378, 1531

Kim, S. et al. 2014, submitted to ApJ

Lee, J., Hahn, O., & Porciani, C. 2009, ApJ, 705, 1469

Lee, J., Rey, S.-C., & Kim, S. 2014, ApJ, 791, 15

Libeskind, N. I., Cole, S., Frenk, C. S., Okamoto, T., & Jenkins, A. 2007, MNRAS, 374, 16

Libeskind, N. I., Hoffman, Y., Knebe, A., et al. 2012, MNRAS, 421, L137

Libeskind, N. I., Hoffman, Y., Forero-Romero, J., et al. 2013, MNRAS, 428, 2489

Libeskind, N. I., Hoffman, Y., Steinmetz, M., et al. 2013, ApJ, 766, L15

Lee, J., & Springel, V. 2010, JCAP, 5, 31

Libeskind, N. I., Hoffman, Y., & Gottlöber, S. 2014, MNRAS, 441, 1974

Libeskind, N. I., Knebe, A., Hoffman, Y., & Gottloeber, S. 2014, arXiv:1407.0394

Park, C., & Choi, Y.-Y. 2005, ApJ, 635, L29

Park, C., & Choi, Y.-Y. 2009, ApJ, 691, 1828

Platen, E., van de Weygaert, R., & Jones, B. J. T. 2008, MNRAS, 387, 128

Sales, L., & Lambas, D. G. 2004, MNRAS, 348, 1236

Springel, V., White, S. D. M., Jenkins, A., et al. 2005, Nature, 435, 629

Tegmark, M., et al. 2004, ApJ, 606, 702

Tempel, E., Libeskind, N. I., Hoffman, Y., Liivamägi, L. J., & Tamm, A. 2014, MNRAS, 437, L11

Wang, H. Y., Jing, Y. P., Mao, S., & Kang, X. 2005, MNRAS, 364, 424

Wang, H., Mo, H. J., Jing, Y. P., et al. 2009, MNRAS, 394, 398

Wang, H., Mo, H. J., Yang, X., & van den Bosch, F. C. 2012, MNRAS, 420, 1809

Wang, Y. O., Lin, W. P., Kang, X., et al. 2014, ApJ, 786, 8

Yang, X., van den Bosch, F. C., Mo, H. J., et al. 2006, MNRAS, 369, 1293

Zentner, A. R., Kravtsov, A. V., Gnedin, O. Y., & Klypin, A. A. 2005, ApJ, 629, 219

Zhang, Y., Yang, X., Faltenbacher, A., et al. 2009, ApJ, 706, 747

Zhang, Y., Yang, X., Wang, H., et al. 2013, ApJ, 779, 160

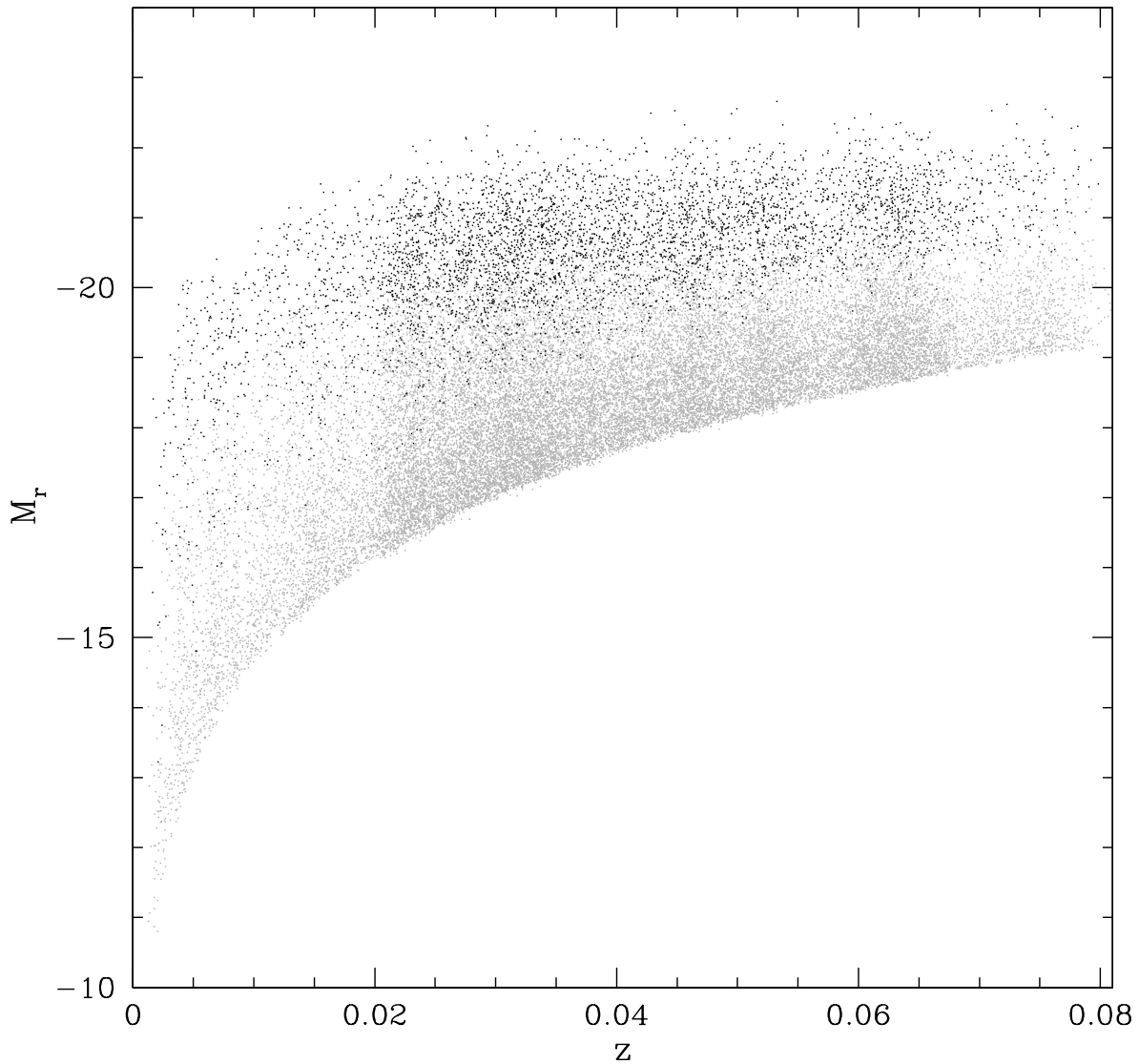


Fig. 1.— Absolute r -band magnitudes of the isolated host galaxies (black dots) and their satellites (grey dots) from the SDSS DR7 as a function of the redshift. For visibility, only those isolated galactic systems with five or more satellites are shown.

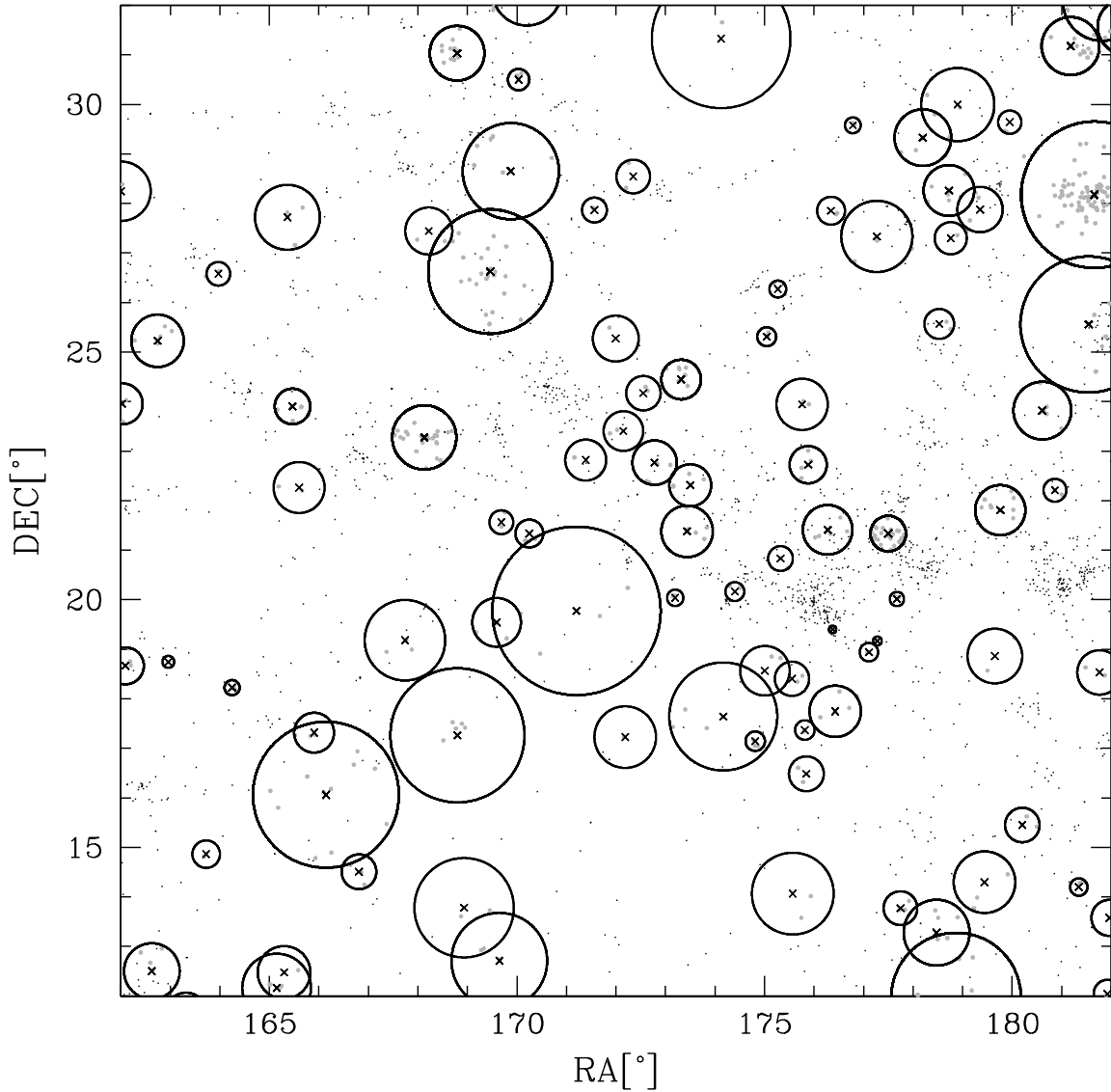


Fig. 2.— Illustration of how to identify the satellites (grey dots) around the isolated host galaxies (cross) in the plane of sky spanned by the right ascension (RA) and declination (DEC) in unit of degree at redshifts of $0.02 \leq z \leq 0.03$. The radii of the circles around the isolated host galaxy represent the maximum separation distances to their satellites.

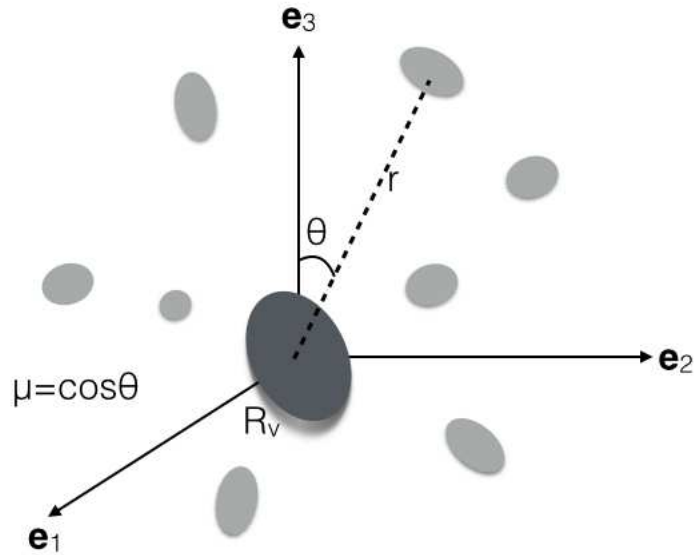


Fig. 3.— Three dimensional spatial distribution of the galactic satellites (pale gray ellipses) located at distances r from the their isolated host (a dark gray ellipse at the center) with a virial radius R_v in the principal frame of the velocity shear tensor determined at the host center. The alignment measure is defined as the mean value of the cosines of the angles $\cos \theta$ between the satellite positions and the principal axes of the velocity shear tensor, $\{\hat{\mathbf{e}}_i\}$, averaged the all galactic satellites.

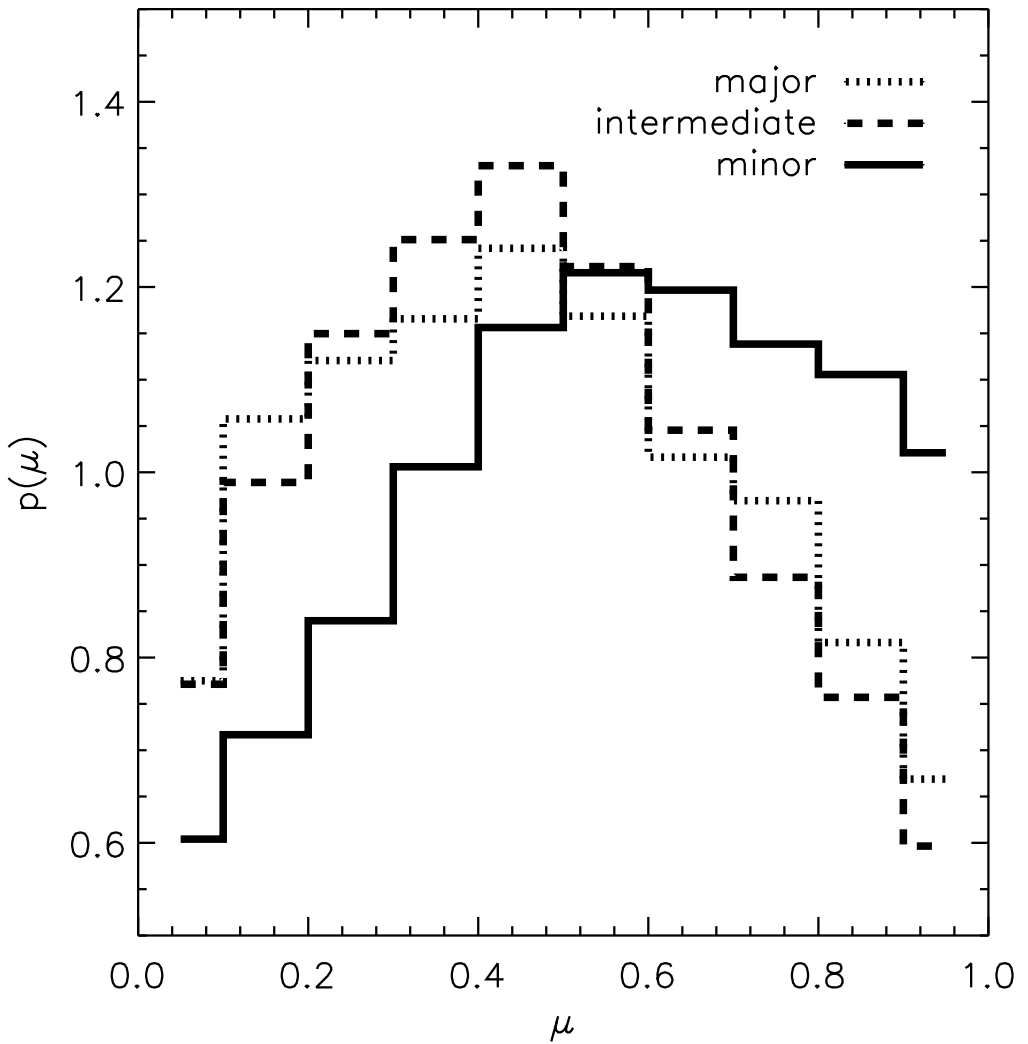


Fig. 4.— Probability density distributions of the alignment measures, μ , between the satellite positions and the major, intermediate, and minor eigen directions of the local velocity shear tensors as dotted, dashed and solid lines, respectively.

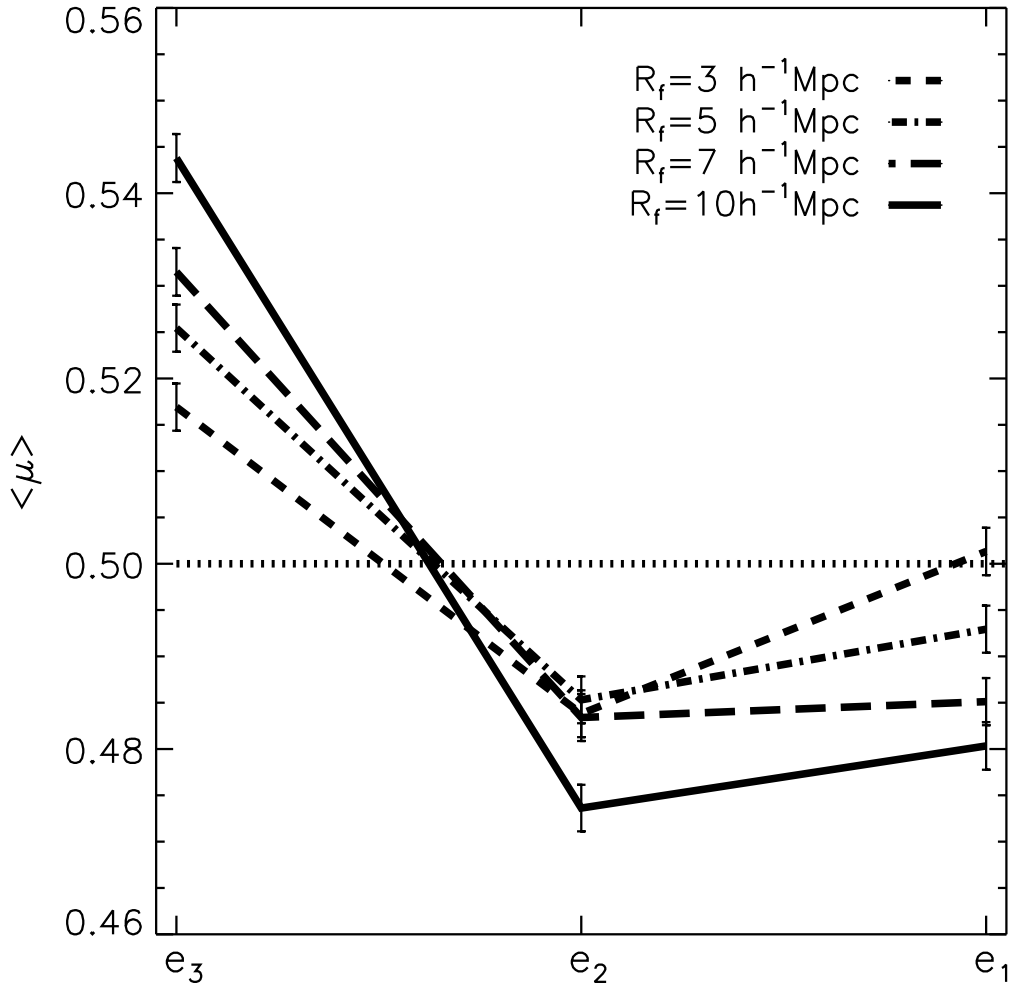


Fig. 5.— Ensemble averages of the alignment measures μ for four different cases of the filtering scale ($R_f = 3, 5, 7$ and $10 h^{-1}\text{Mpc}$ as dotted, dashed, dot-dashed and solid lines, respectively) . The averages are taken over all isolated galactic systems which have one or more satellites. The first, second and third bins correspond to the alignments with the minor (e_3), intermediate (e_2) and major (e_1) principal axes of the local velocity shear, respectively.

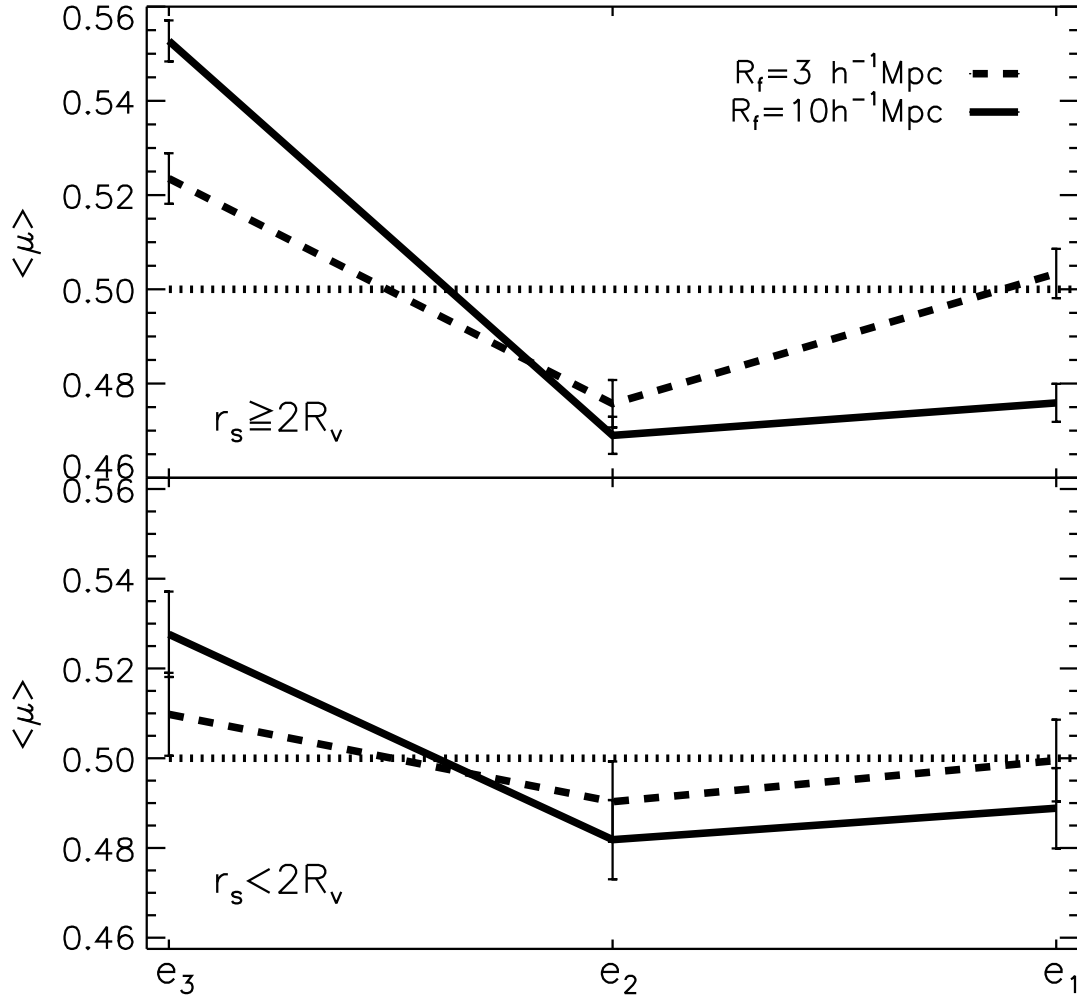


Fig. 6.— Alignment measure determined by using only those satellites with $r \geq 2R_v$ ($r \leq 2R_v$) in the top (bottom) panel where r is the three dimensional separation distance between the host and its satellite and R_v is the tangential virial radius of the host. In each panel, the solid and dashed line represent two different cases of R_f are shown: ($R_f = 3 h^{-1}\text{Mpc}$ and $10 h^{-1}\text{Mpc}$, respectively).

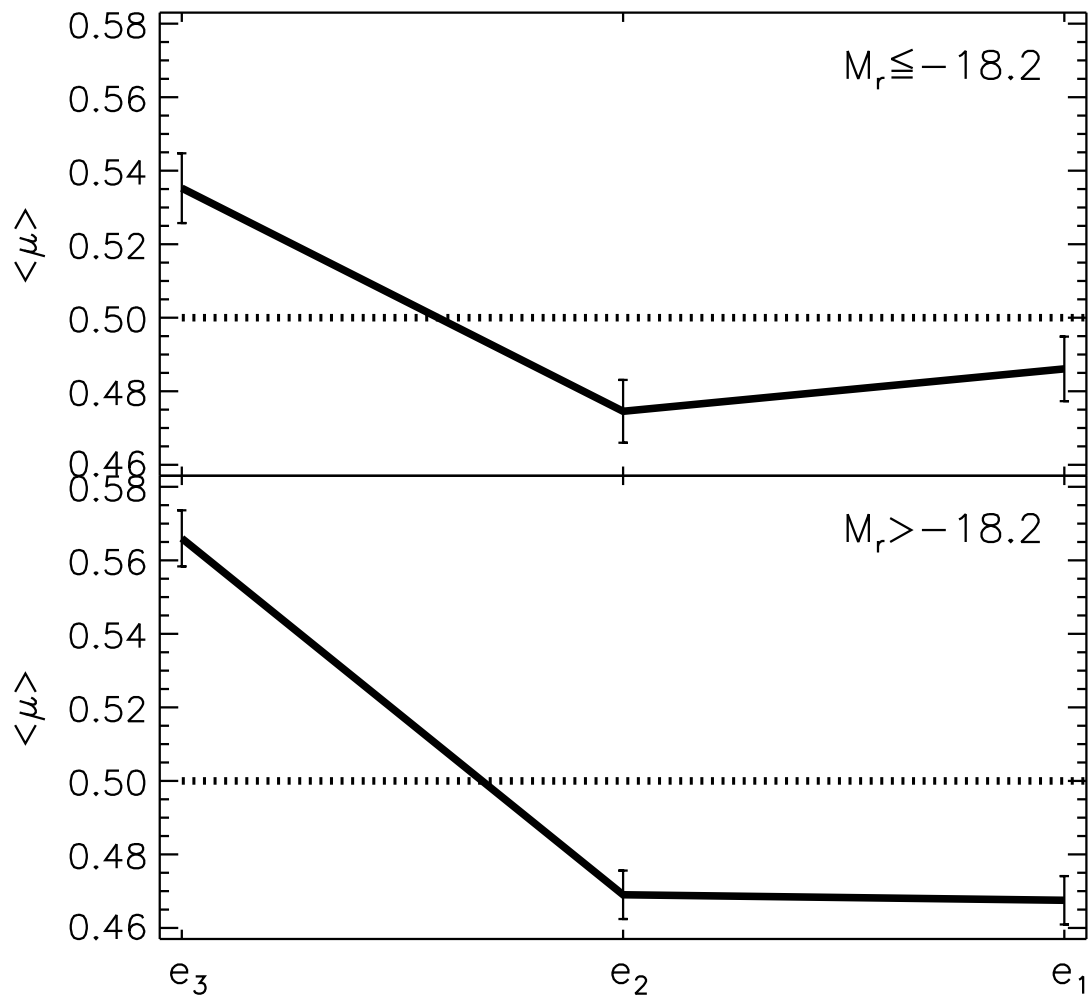


Fig. 7.— Alignment measure determined by using only those satellites with the r -band absolute magnitude $M_r \leq -18.2$ ($M_r > -18.2$) in the top (bottom) panel.

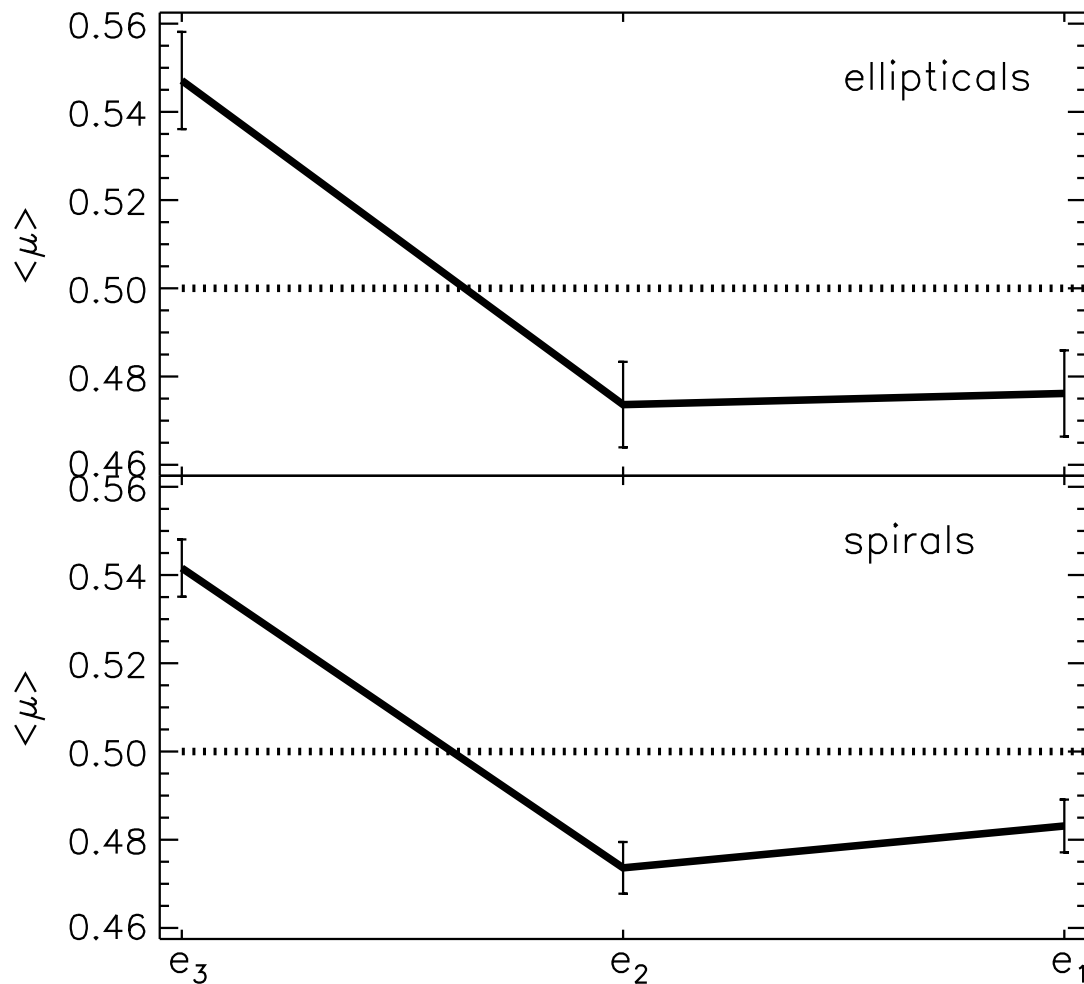


Fig. 8.— Alignment measure determined by using only those elliptical (spiral) satellites in the top (bottom) panel.

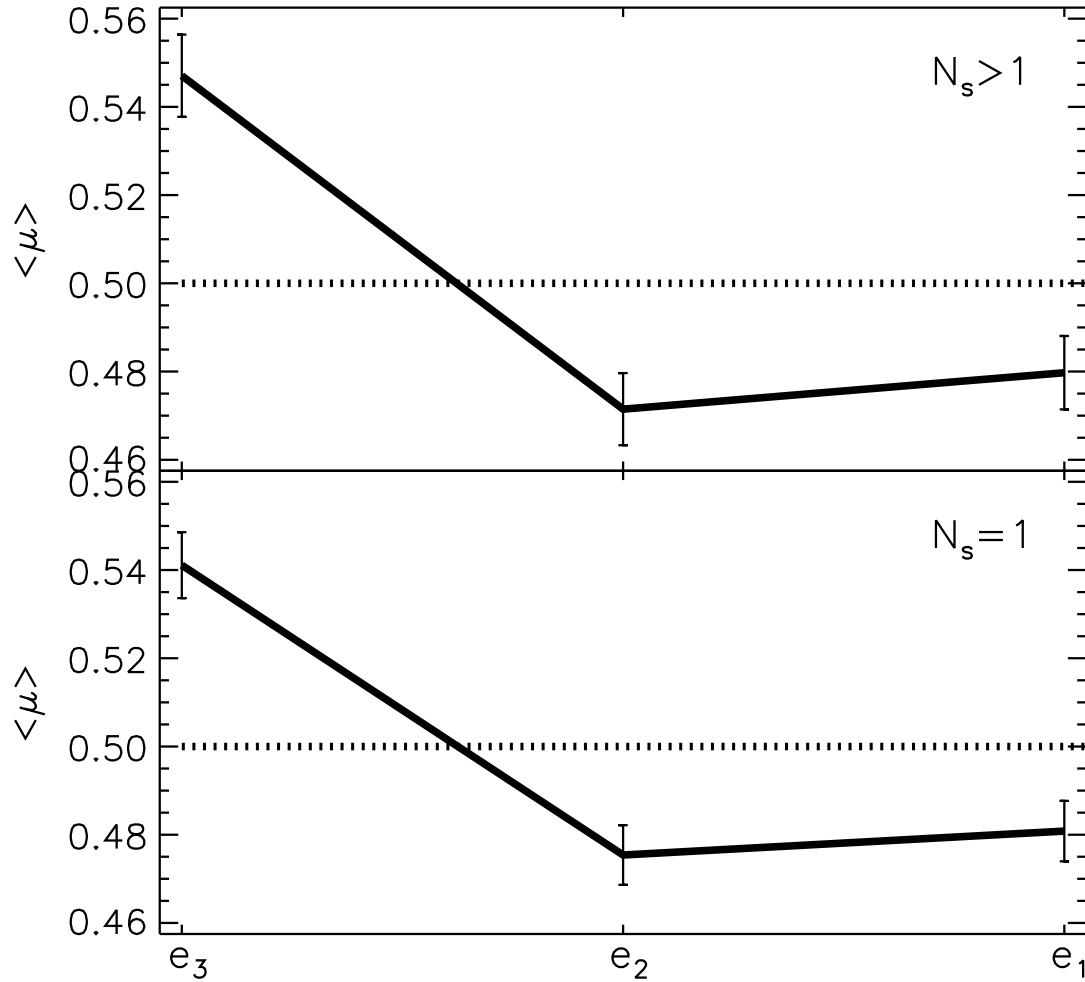


Fig. 9.— Alignment measure averaged only over those systems with $N_s \geq 2$ ($N_s < 2$) in the top (bottom) panel where N_s is the number of the satellites in the system.

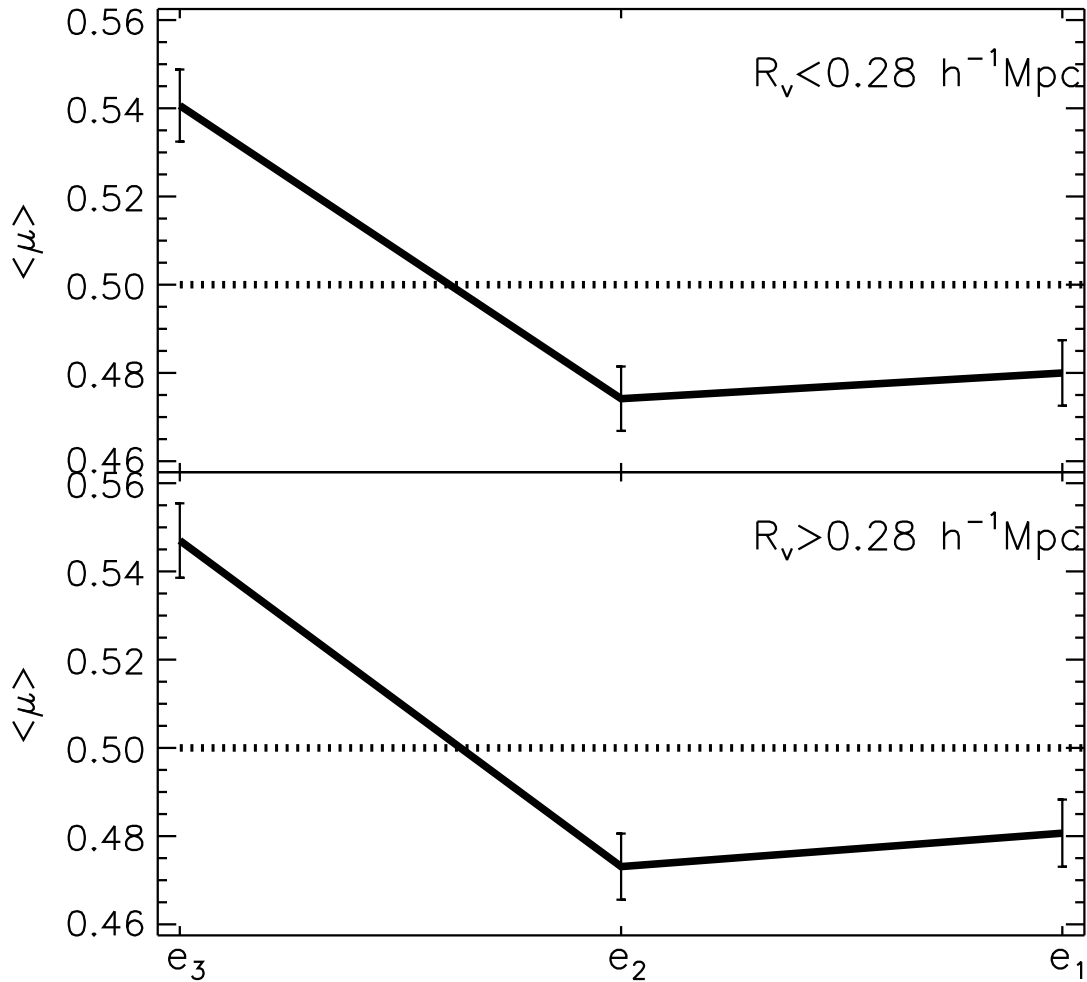


Fig. 10.— Alignment measure averaged only over those systems with $R_v < 0.28 h^{-1}\text{Mpc}$ ($R_v \geq 0.28 h^{-1}\text{Mpc}$) in the top (bottom) panel where R_v is the tangential virial radius of an isolated host galaxy and the value of $0.28 h^{-1}\text{Mpc}$ is its median from all of the isolated host galaxies.

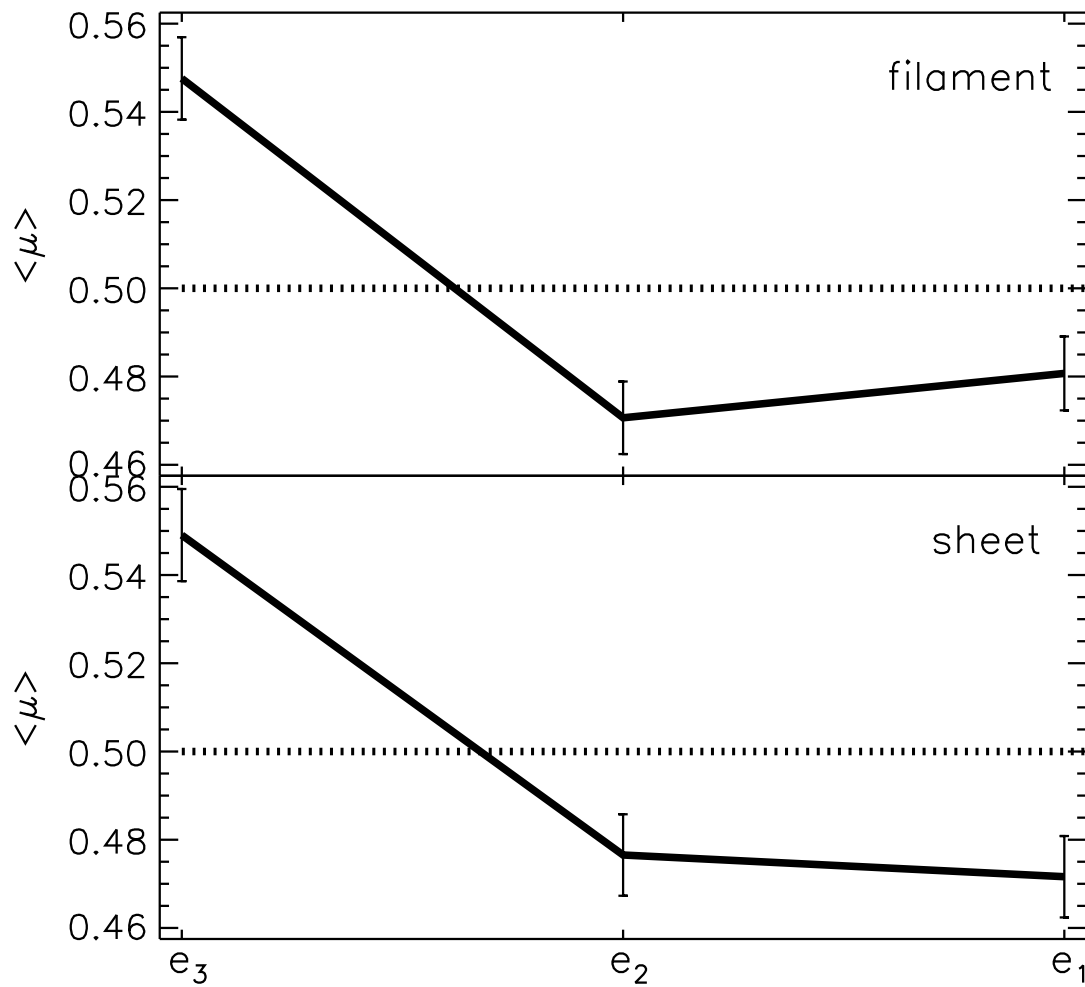


Fig. 11.— Alignment measure averaged only over those systems located in the filament (sheet) environments in the top (bottom) panel.

Table 1. Absolute r -band magnitude, tangential virial radius, mean number of the satellites of the isolated hosts within the local volume

M_r	R_v (h^{-1} Mpc)	\bar{N}_s
[-22.66, -12.85]	[0.027, 0.687]	2.6